Available online at www.sciencedirect.com
SCIENCE DIRECT®
Journal of Colloid and Interface Science 277 (2004) 184–201
JOURNAL OF Colloid and Interface Science
www.elsevier.com/locate/jcis

# Free energy balance for three fluid phases in a capillary of arbitrarily shaped cross-section: capillary entry pressures and layers of the intermediate-wetting phase

M.I.J. van Dijke [a,*], M. Lago [b], K.S. Sorbie [a], M. Araujo [c]

[a] *Institute of Petroleum Engineering, Heriot–Watt University, Edinburgh, UK*
[b] *Applied Marine Physics Department, RSMAS, University of Miami, USA*
[c] *Escuela de Fisica, Universidad Central de Venezuela, Caracas, Venezuela*

Received 26 November 2003; accepted 18 May 2004

Available online 5 June 2004

**Abstract**

In this work we derive rigorously the free energy balance for three fluid phases in a straight capillary of arbitrarily shaped cross-section. This balance is then used to derive the general equation for the capillary entry pressures of all possible two-phase and three-phase displacements. Moreover, the equation provides the criterion determining the existence of layers of the intermediate-wetting phase separating the wetting and non-wetting phases in the corners or cavities of a capillary, by also treating the spreading of such layers as a capillary displacement. For a number of combinations of interfacial tensions and contact angles, illustrating all the different relevant situations, we calculate the criteria for spreading of such a layer in the corner of a capillary with polygonal cross-section. In a capillary with a cross-section in the shape of an isosceles triangle of varying corner size, these criteria are used to determine the unique capillary entry pressures for piston-like displacement from alternative solutions of the general equation. These solutions relate to displacements in the presence or absence of layers in the various differently sized corners.
© 2004 Elsevier Inc. All rights reserved.

*Keywords:* Three-phase; Free energy; Capillary; Irregular cross-section; Displacement; Entry pressure; Intermediate-wetting layer

## 1. Introduction

Pore-scale modelling of multi-phase flow processes is mainly determined by capillary forces, in particular by so-called capillary entry pressures or threshold pressures. The capillary entry pressure determines the pressure difference that is necessary for one (bulk) phase to displace another (bulk) phase in a capillary. In a capillary shaped as a straight cylinder the Young–Laplace equation provides a simple expression for the capillary entry pressure, based on the assumptions that only one phase can occupy a given cross-section and that the interface between the two phases has a known (spherical) shape. However, in irregularly shaped capillaries these assumptions are usually not valid as the more wetting phase tends to be present in corners or cavities of the pore cross-section, even when more non-wetting phases are present in the centre of the cross-section. Furthermore, for most pore shapes the shape of the bulk–bulk interface is difficult to determine.

Despite the irregularity of the pore cross-sections Mayer and Stowe [1] and Princen [2–4] have developed a method (referred to as the MS-P method) that can be applied to determine the capillary entry pressure for two-phase flow in straight capillary of irregular cross-section. Many researchers after them have applied this method to study particular cross-sectional shapes and have extended the method to pores of arbitrary wettability conditions. The corresponding references have been collected by Lago and Araujo [5], who themselves have considered pores of general polygonal cross-section and, more recently, pores with curved sides [6]. The MS-P method is based on the variation of free energy for a long capillary in which two phases are separated by a bulk–bulk interface, as well as by interfaces in the corners and cavities of the pore cross-section.

* Corresponding author. Fax: +44-(0)-131-4513165.
*E-mail address:* rink@pet.hw.ac.uk (M.I.J. van Dijke).

0021-9797/$ – see front matter © 2004 Elsevier Inc. All rights reserved.
doi:10.1016/j.jcis.2004.05.021

Recently, van Dijke and Sorbie [7] have extended the two-phase MS-P theory to systems of three fluid phases. They considered the capillary entry pressures for displacement of two bulk phases in a capillary, where also the remaining third phase is present in the corners and cavities. An equation was formulated from which the capillary entry pressures for all possible two-phase and three-phase piston-like displacements, relevant to pore-scale modelling, can be derived. Van Dijke and Sorbie illustrated the generality of the method by deriving the entry pressures for pores of various polygonal cross-sectional shapes, in particular for a rhombus, as the latter shape has in general two pairs of unequally sized corners, which may lead to different corner phase occupancies. In most cases where three phases are present in one capillary, the entry pressures for displacement between the two bulk phases can be shown to depend on the pressure in the remaining third phase. In this framework, also the situation was discussed where in a given cross-section all three phases are present, i.e., where the intermediate-wetting phase resides as a thick layer, separated by two different interfaces, between the wetting and the non-wetting phase. This situation markedly affects the capillary entry pressures.

The presence of these intermediate-wetting layers has been observed experimentally [8–10] and predicted theoretically [8,11,12]. Fenwick and Blunt [11] and Firincioglu et al. [12] have only provided geometrical criteria, which can be seen as necessary conditions for the existence of the intermediate-wetting layers. Dong et al. [8] used a free energy approach to derive a sufficient criterion for the existence of the layers in terms of the pressure differences between the phases, which supposedly needed to be calculated numerically. In this paper, we show that the sufficient condition, i.e., pressure combinations, for the existence of the layers follows from the same general equation as is used to derive the three-phase capillary entry pressures. These pressure combinations are then restricted by the mentioned geometrical criterion to determine uniquely the presence of these intermediate-wetting layers.

In Section 2 we derive rigorously the free energy balance for the presence of three fluid phases in a closed system with rigid walls. In the present case, we consider the system to be a capillary network, in which we look at phase volume variations in one capillary only, or, even simpler, we consider a single closed capillary. In Section 3 we show how this balance is applied to find the equation necessary to determine the capillary entry pressures for all possible two-phase and three-phase displacements. Moreover, we show that this equation also leads to the existence criterion for the intermediate-wetting layers. The equation is valid for arbitrary cross-sectional geometries, but to illustrate our ideas best, we apply it to pores of polygonal cross-section. Therefore, we state the corresponding relations for the corner geometries in Section 4 and we work out explicitly the criterion for the existence of an intermediate-wetting layer in such a corner. In Section 5, we give numerical examples of the layer criterion and the various capillary entry pressures in a pore with cross-section in the shape of an isosceles triangle for varying corner sizes. We show how the layer criterion distinguishes between alternative solutions for the capillary entry pressures, as it determines the conditions, i.e., pressure combinations, under which intermediate-wetting layers are present in the various corners. In Appendix A we revisit the analysis of Dong et al. [8] for the existence of layers to show that their and our derivation lead to the same criterion.

## 2. Free energy balance for three phases in a closed system

When three fluid phases are present in a closed system with rigid walls the total free energy differential $dF_T$ is given by the sum of differentials,

$$dF_T = \sum_{i=1,2,3} dF_i + \sum_{i=1,2,3} dF_{is} + \sum_{ij=12,13,23} dF_{ij}, \qquad (1)$$

where the single numbered indices refer to the fluid phases. The double indices refer to interfaces between the fluid phases mutually, as well as between the fluid phases and the solid phase $s$ associated with the walls. Assuming that the system is in thermal equilibrium with its surroundings, the equilibrium condition for the variation in (Helmholtz) free energy is $dF_T = 0$ [13,14].

Because of constancy of temperature and chemical potential, the differentials associated with the individual phases $dF_i$ in Eq. (1) can be written as

$$dF_i = -P_i\,dV_i, \qquad (2)$$

where $dV_i$ denotes the phase volume variations and $P_i$ denotes the (constant) pressure of fluid phase $i$. Assuming very thin interfaces between the phases, the differentials associated with the fluid–solid and fluid–fluid interfaces, $dF_{is}$ and $dF_{ij}$ respectively, can be written as

$$dF_{is} = \sigma_{is}\,dA_{is}, \qquad dF_{ij} = \sigma_{ij}\,dA_{ij}, \qquad (3)$$

where $dA_{is}$ and $dA_{ij}$ denote variations in the corresponding surface areas. Furthermore, $\sigma_{is}$ denotes the surface tension between fluid phase $i$ and the solid $s$ and $\sigma_{ij}$ denotes the interfacial tension between fluid phases $i$ and $j$.

Hence, the equilibrium condition $dF_T = 0$ leads to the balance of virtual work produced by phase volume changes and the virtual work associated with the changes in interfacial areas for three fluids:

$$-\sum_{i=1,2,3} P_i\,dV_i + \sum_{i=1,2,3} \sigma_{is}\,dA_{is} + \sum_{ij=12,13,23} \sigma_{ij}\,dA_{ij} = 0. \qquad (4)$$

Because of the rigid solid phase, the total fluid phase volume and the total fluid–solid surface area remain constant, i.e.,

$$\sum_{i=1,2,3} dV_i = 0, \qquad \sum_{i=1,2,3} dA_{is} = 0. \qquad (5)$$

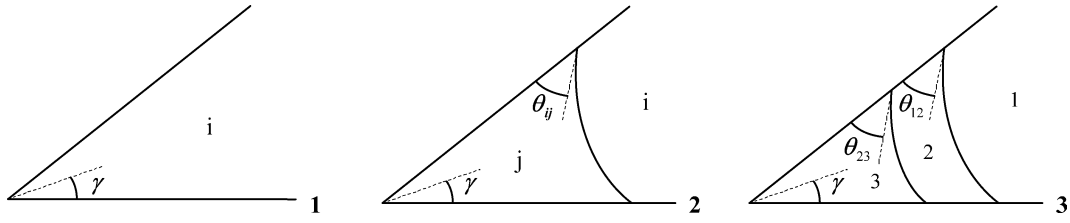


Fig. 1. Possible three-phase configurations in the corner of a pore illustrated by a corner with straight walls and half angle $\gamma$. In configuration 2 one corner fluid–fluid interface (AM) is present separating the more non-wetting phase $i$ from the more wetting phase $j$. In configuration 3 a layer of the intermediate-wetting phase 2 separates phases 1 and 3 and is surrounded by both a 12 and a 23 AM. Additionally, the fluid–fluid contact angles $\theta_{ij}$ are indicated.

We use these constraints in Section 3, where we invoke an infinitely small displacement of the phases to derive the capillary entry pressures in a capillary with rigid walls.

Further, in the presence of pore walls contact angles $\theta_{ij}$, $ij = 12, 13, 23$, can be defined, measured through phase $j$, which obey Young's equation

$$\sigma_{is} - \sigma_{js} = \sigma_{ij} \cos\theta_{ij}. \tag{6}$$

For the three phase pairs Eq. (6) combines into the equation of Bartell and Osterhof [15],

$$\sigma_{13} \cos\theta_{13} - \sigma_{23} \cos\theta_{23} = \sigma_{12} \cos\theta_{12}. \tag{7}$$

Notice, that the introduction of contact angles allows the balance (4) to be valid for systems of arbitrary wettability and we choose the numbering of the phases (from non-wetting to intermediate-wetting to wetting as 1, 2 and 3) based on the values of the contact angles. As a result, we can assume without loss of generality that $0 \leqslant \theta_{ij} \leqslant \pi/2$ for $ij = 12, 13, 23$, with the subscripts in this order.

Using Eqs. (5) and (6), we may eliminate any one of the terms $dV_i$ and $dA_{is}$ from the energy balance (4), for example $dV_3$ and $dA_{3s}$, to obtain the slightly more compact form

$$\begin{aligned} &-P_{13}\,dV_1 - P_{23}\,dV_2 + \sigma_{12}\,dA_{12} \\ &\quad + \sigma_{13}(dA_{13} + \cos\theta_{13}\,dA_{1s}) \\ &\quad + \sigma_{23}(dA_{23} + \cos\theta_{23}\,dA_{2s}) = 0, \end{aligned} \tag{8}$$

where we have also introduced $P_{ij} = P_i - P_j$ for $ij = 12, 23$, which satisfies by definition

$$P_{13} = P_{12} + P_{23}. \tag{9}$$

Notice that the formulation of Eq. (8) is slightly "asymmetric" as, for example, the term involving $\sigma_{12}$ is different from the terms involving $\sigma_{13}$ and $\sigma_{23}$. Therefore, although Eq. (8) is as general as Eq. (4), we use the latter as the starting point for our derivation in the next section.

## 3. Three-phase capillary entry pressures

As described by van Dijke and Sorbie [7], capillary entry pressures for piston-like displacement of two phases in a pore in the presence of a third phase can be obtained using a free energy balance. The work of van Dijke and Sorbie is a generalisation of the method by Mayer and Stowe [1] and Princen [2–4], the MS-P method, who derived capillary entry pressures in two-phase flow. In this method, it is assumed that in a long capillary a main terminal meniscus (MTM) exists, which separates longitudinal sections of the capillary with different cross-sectional phase configurations. In the cross-sections far away from the MTM the interfaces between the fluid phases form arc menisci (AM) with radii of curvature $r_{ij}$. The crux of the MS-P method lies in comparing the effective radius of curvature at the MTM with the radii of the AMs. Broadly speaking, if in a cross-section all three phases are present, the non-wetting phase tends to reside in the centre or bulk of the capillary, the wetting phase resides in the narrower parts or corners and the intermediate-wetting phase forms layers between these phases. The phases are separated by the AMs. Also if two phases are present, the more wetting phase resides in the narrower parts of the capillaries. To analyse the cross-sectional phase occupancies it is sufficient to identify the AMs in the various corners and cavities.

For a capillary of polygonal cross-section van Dijke and Sorbie [7] have identified all possible cross-sectional configurations from the occupancies in the individual corners of the capillary, where the latter are summarised in Fig. 1. Also in the general case, where in a cross-section the pore walls are not straight, the essence is to identify the AMs in the narrower parts of the cross-section as demonstrated for two-phase flow by Mayer and Stowe [1] and Princen [2–4] and, more recently, by Lago and Araujo [6]. The corner occupancies constitute the phase occupancy in an entire cross-section, of which examples are given for an arbitrary triangle in Fig. 2a. Observe that there is one bulk phase present in each cross-section, i.e., phase 1 at $a$ and phase 2 at $b$, but that in the various corners different phases are present, i.e., different AMs. In Section 4.1 we discuss the precise conditions for the presence of the various AMs for a polygonal cross-section.

Combination of cross-sections $a$ and $b$ of Fig. 2a for a slice along a long capillary, separated by the MTM, is shown in Fig. 2b. For this example, at the MTM three different fluid–fluid interfaces are present, although their precise shape is unknown due to the irregular shape of the cross-section. However, according to the Laplace equation

$$P_{ij} = \frac{\sigma_{ij}}{r_{ij}} \tag{10}$$

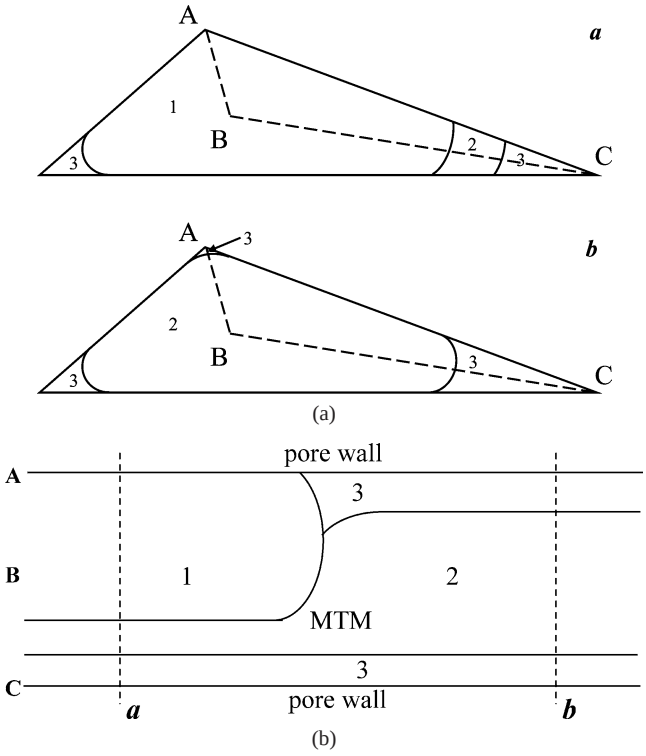


Fig. 2. (a) Cross-sections of a triangular capillary with possible phase configurations with either phase 1 or phase 2 as bulk phase. (b) Section through A–B–C of part (a) along the length of the capillary with three fluid phases. The cross-sections $a$ and $b$ in part (b) are taken at locations where the fluid–fluid interfaces can be assumed to be parallel to the pore walls.

the effective radii of curvature $r_{ij}$, $ij = 12, 13, 23$, for these interfaces can be defined in terms of the phase pressure differences. To determine these radii, we consider the fluid configuration at thermodynamic equilibrium. At equilibrium, the effective radii at the MTM are equal to those for the AMs, if present, of which the actual radius of curvature is equal to $r_{ij}$. Furthermore, because the phase pressures are constant throughout the system, AMs of the same fluid–fluid combination have the same radius of curvature on either side of the MTM.

### 3.1. General derivation

The free energy balance for such a three-phase configuration, given by Eq. (4), is based on a small variation of the phase volumes. In a system composed of a sufficiently long closed capillary, we may assume that small variations of the phase volumes lead to changes in the lengths of the fluid distributions only and that the shape of the MTMs remain constant. We associate these length variations with a small displacement of the MTM in the direction along the length of the capillary, say $dx$.

Hence, taking $dx$ directed from cross-section $a$ towards cross-section $b$, the volume and area variations in Eq. (4) can be expressed as

$$dV_i = (A_i|_a - A_i|_b)\,dx \quad \text{for } i = 1, 2, 3, \tag{11a}$$

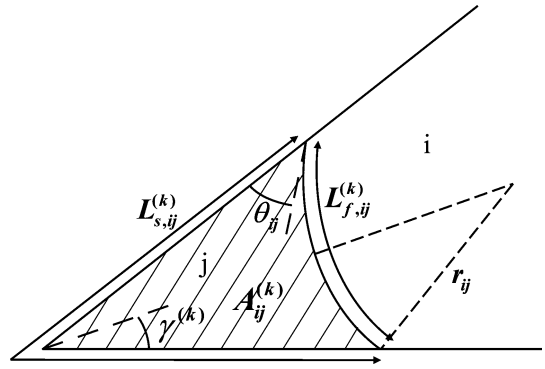


Fig. 3. Cross-sectional area $A_{ij}^{(k)}$ occupied by phase $j$ in corner $\alpha$ in the presence of bulk phase $i$. The lengths of the surrounding fluid–solid and fluid–fluid contact lines are indicated as $L_{s,ij}^{(k)}$ and $L_{f,ij}^{(k)}$, respectively.

$$dA_{is} = (L_{is}|_a - L_{is}|_b)\,dx \quad \text{for } i = 1, 2, 3, \tag{11b}$$

$$dA_{ij} = (L_{ij}|_a - L_{ij}|_b)\,dx \quad \text{for } ij = 12, 13, 23, \tag{11c}$$

where $A_i|_z$ for $z = a, b$ denotes the area of cross-section $z$ that is occupied by phase $i$. Similarly, $L_{is}|_z$ denotes the length of the contact-line between phase $i$ and the solid, while $L_{ij}|_z$ denotes the length of the contact-line between phases $i$ and $j$ in cross-section $z$. Notice, that $A_i|_z$, $L_{is}|_z$ and $L_{ij}|_z$ are equal to zero if the corresponding volumes and interfaces are not present in the indicated cross-section. For example, for the phase configuration of Fig. 2b $dA_{12} = L_{12}|_a\,dx$, $dA_{13} = L_{13}|_a\,dx$ and $dA_{23} = (L_{23}|_a - L_{23}|_b)dx$. Observe that Eqs. (11a) and (11b) are consistent with the conservation equations (5), since

$$\sum_{i=1,2,3} A_i|_z = A \quad \text{and} \quad \sum_{i=1,2,3} L_{is}|_z = L_s \quad \text{for } z = a, b,$$

where $A$ and $L_s$ are the total area and perimeter of the cross-section, respectively.

Substitution of Eqs. (11) in Eq. (4) and considering that the displacement $dx$ is arbitrary yields

$$\left\{-\sum_{i=1,2,3} P_i A_i + \sum_{i=1,2,3} \sigma_{is} L_{is} + \sum_{ij=12,13,23} \sigma_{ij} L_{ij}\right\}_a - \left\{-\sum_{i=1,2,3} P_i A_i + \sum_{i=1,2,3} \sigma_{is} L_{is} + \sum_{ij=12,13,23} \sigma_{ij} L_{ij}\right\}_b = 0, \tag{12}$$

which may be viewed as a balance of the forces acting on either side of the MTM.

For convenience, we write $A_i$ in terms of the total area $A$ of the cross-section and the corner areas $A_{ij}^{(k)}$, which are bounded by the AM between phases $i$ and $j$ in a particular corner $k$. Similarly, we write the fluid–solid contact-line lengths in terms of the total perimeter of the cross-section $L_s$ and the fluid–solid contact-line lengths in the corner $L_{s,ij}^{(k)}$. The corner notation is illustrated in Fig. 3 for a simple corner with straight walls. The advantage of this notation is that

we only have to deal with the constant total area and perimeter, separate from the corner quantities, which vary with the indicated AM only. For example, $L_{s,ij}^{(k)}$ depends on the AM between phases $i$ and $j$ only, parameterised by the radius of curvature $r_{ij}$ and the contact angle $\theta_{ij}$. In Section 4.1 we work out the expressions for these corner quantities for a simple corner with straight walls.

In general, assuming that we have a cross-section with $n$ corners or cavities, where possible AMs can be identified, we can express the areas and contact-line lengths as

$$\begin{aligned}
A_1|_z &= A\delta_{1,z} - \sum_{k=1}^{n}\bigl(A_{12}^{(k)}\delta_{12,z}^{(k)} + A_{13}^{(k)}\delta_{13,z}^{(k)}\bigr),\\
A_2|_z &= A\delta_{2,z} - \sum_{k=1}^{n}\bigl(A_{23}^{(k)}\delta_{23,z}^{(k)} - A_{12}^{(k)}\delta_{12,z}^{(k)}\bigr),\\
A_3|_z &= A\delta_{3,z} - \sum_{k=1}^{n}\bigl(-A_{13}^{(k)}\delta_{13,z}^{(k)} - A_{23}^{(k)}\delta_{23,z}^{(k)}\bigr), \qquad (13a)\\
L_{1s}|_z &= L_s\delta_{1,z} - \sum_{k=1}^{n}\bigl(L_{s,12}^{(k)}\delta_{12,z}^{(k)} + L_{s,13}^{(k)}\delta_{13,z}^{(k)}\bigr),\\
L_{2s}|_z &= L_s\delta_{2,z} - \sum_{k=1}^{n}\bigl(L_{s,23}^{(k)}\delta_{23,z}^{(k)} - L_{s,12}^{(k)}\delta_{12,z}^{(k)}\bigr),\\
L_{3s}|_z &= L_s\delta_{3,z} - \sum_{k=1}^{n}\bigl(-L_{s,13}^{(k)}\delta_{13,z}^{(k)} - L_{s,23}^{(k)}\delta_{23,z}^{(k)}\bigr), \qquad (13b)\\
L_{ij}|_z &= \sum_{k=1}^{n} L_{f,ij}^{(k)}\delta_{ij,z}^{(k)} \quad \text{for } ij = 12, 13, 23. \qquad (13c)
\end{aligned}$$

In Eqs. (13) we have used the following indicator notation convention, similar to [5]:

$$\delta_{i,z} = \begin{cases} 1 & \text{if phase } i \text{ present at } z,\\ 0 & \text{otherwise,}\end{cases} \qquad (14a)$$

$$\delta_{ij,z}^{(k)} = \begin{cases} 1 & \text{if } ij \text{ AM present in corner } k \text{ at } z,\\ 0 & \text{otherwise.}\end{cases} \qquad (14b)$$

Notice, that $\delta_{i,z}$ refers to bulk phase occupancy and $\delta_{ij,z}^{(k)}$ to corner occupancy. Furthermore, since each cross-section contains only one bulk phase, the $\delta_{i,z}$ satisfy $\sum_{i=1,2,3}\delta_{i,z} = 1$. On the other hand, there is no similar constraint for the $\delta_{ij,z}^{(k)}$, since zero, one or even two AMs may be present in a given corner. However, the presence of AMs, therefore the values of $\delta_{ij,z}^{(k)}$, is constrained by the type of bulk phase, as indicated in Section 3.2 below.

Using Eqs. (13) the individual summations in Eq. (12) relating to one cross-section $z$ transform into

$$\begin{aligned}
-\sum_{i=1,2,3} P_i A_i|_z &= -\sum_{i=1,2,3} P_i A\delta_{i,z}\\
&\quad + \sum_{k=1}^{n}\sum_{ij=12,13,23} P_{ij} A_{ij}^{(k)}\delta_{ij,z}^{(k)}, \qquad (15a)\\
\sum_{i=1,2,3} \sigma_{is} L_{is}|_z &= \sum_{i=1,2,3} \sigma_{is} L_s\delta_{i,z}\\
&\quad - \sum_{k=1}^{n}\sum_{ij=12,13,23} \sigma_{ij}\cos\theta_{ij} L_{s,ij}^{(k)}\delta_{ij,z}^{(k)}, \qquad (15b)\\
\sum_{ij=12,13,23} \sigma_{ij} L_{ij}|_z &= \sum_{k=1}^{n}\sum_{ij=12,13,23} \sigma_{ij} L_{f,ij}^{(k)}\delta_{ij,z}^{(k)}, \qquad (15c)
\end{aligned}$$

where we have used the definition $P_{ij} = P_i - P_j$ in relation (15a) and Eq. (6) in relation (15b), similar to the derivation of Eq. (8). Furthermore, the difference of the bulk phase terms in relations (15a) and (15b) for the two cross-sections $a$ and $b$ can be expressed as

$$\begin{aligned}
&-\sum_{i=1,2,3}(P_i A - \sigma_{is} L_s)\delta_{i,a} + \sum_{i=1,2,3}(P_i A - \sigma_{is} L_s)\delta_{i,b}\\
&\quad = -\sum_{ij=12,13,23}(P_{ij} A - \sigma_{ij}\cos\theta_{ij} L_s)\delta_{ij,ab}, \qquad (16)
\end{aligned}$$

where $\delta_{ij,ab}$ denotes the indicator function for the combination of bulk phases on either side of the MTM, defined as

$$\delta_{ij,ab} = \begin{cases} 1 & \text{if bulk phase } i \text{ present at } a \text{ and}\\ & \text{bulk phase } j \text{ present at } b,\\ -1 & \text{if bulk phase } j \text{ present at } a \text{ and}\\ & \text{bulk phase } i \text{ present at } b.\end{cases} \qquad (17)$$

To arrive at a compact canonical form of the energy balance (12), we use the geometrical functions [7]

$$\begin{aligned}
g(r,\theta) &= \frac{A}{r} - \cos\theta\cdot L_s, \qquad (18a)\\
g^{(k)}(r,\theta) &= \frac{A^{(k)}(r,\theta)}{r} + L_f^{(k)}(r,\theta)\\
&\quad - \cos\theta\cdot L_s^{(k)}(r,\theta), \qquad (18b)
\end{aligned}$$

with $A^{(k)}(r_{ij},\theta_{ij}) = A_{ij}^{(k)}$, $L_s^{(k)}(r_{ij},\theta_{ij}) = L_{s,ij}^{(k)}$, $L_f^{(k)}(r_{ij},\theta_{ij}) = L_{f,ij}^{(k)}$. Relation (18a) only involves the geometry of the total cross-section and relation (18b) relates to the geometry in the corners. Using Eq. (10), we find that with relations (15), (16) and (18) the energy balance (12) is equivalent to

$$\begin{aligned}
&-\sum_{ij=12,13,23}\sigma_{ij} g(r_{ij},\theta_{ij})\delta_{ij,ab}\\
&\quad + \sum_{k=1}^{n}\sum_{ij=12,13,23}\sigma_{ij} g^{(k)}(r_{ij},\theta_{ij})\bigl(\delta_{ij,a}^{(k)} - \delta_{ij,b}^{(k)}\bigr) = 0. \qquad (19)
\end{aligned}$$

Notice that we have eliminated the length of the displacement $dx$, but if we assume that $dx$ is positive, the sign of the left-hand side of Eq. (19) is also the sign of the original free energy variation in Eq. (4).

### 3.2. Application of the general equation

The general equation (19) applies to a straight capillary of any cross-sectional shape where $n$ corners or cavities with possible AMs can be identified. To use this equation

the geometry of the pore cross-section needs to be determined, distinguishing bulk space and corners or cavities, which yield the functions $g$ and $g^{(k)}$, respectively. Identifying these corners for irregularly shaped pores is not always easy, but in general we may define them as parts of the pore space where wetting phase with an associated AM can be present. Then, the pair of bulk phases determines the value of the indicator function $\delta_{ij,ab}$ and for each corner the presence or absence of a particular interface determines the value of the indicator functions $\delta_{ij,z}^{(k)}$.

Equation (19) is the same as Eq. (18) of van Dijke and Sorbie [7] but in a different notation.[1] As outlined in [7], Eq. (19) depends in general on the three radii of curvature for which we have one additional equation, i.e.,

$$\frac{\sigma_{13}}{r_{13}} = \frac{\sigma_{12}}{r_{12}} + \frac{\sigma_{23}}{r_{23}}, \tag{20}$$

which follows from Eqs. (9) and (10). Therefore, Eq. (19) can be reduced to a functional relation between at most two of the radii of curvature. This means that, given one of the radii of curvature, i.e., one pressure difference, the remaining radii can be calculated. In case of different bulk phases on either side of the MTM, the resulting pressure difference between these phases is identified as the capillary entry pressure, which then generally varies with one of the remaining pressure differences.

Using Eqs. (19) and (20) we can derive the capillary entry pressures for displacements related to all possible two-phase and three-phase configurations in a capillary of arbitrary cross-section. Van Dijke and Sorbie [7] have discussed in detail the displacements in capillaries of polygonal cross-section, for all possible combinations of different bulk phases on either side of the MTM. A classification of the different displacements can be made based on the combinations of bulk phases in cross-sections $a$ and $b$, of which there are six, i.e., 12, 13, 23, 11, 22 and 33. It follows easily that the combinations 21, 31 and 32 lead to the same solutions as for 12, 13 and 23, respectively.

As mentioned earlier, the presence of a given bulk phase restricts the number of AMs that can be present in the considered cross-section, since additional phases present in the narrower parts of the capillary must be wetting relative to the bulk phase. This means that bulk phase 3 does not allow any AMs, whereas bulk phase 2 only allows 23 AMs. For bulk phase 1 all three AMs can be present in a given cross-section, although the 23 AM occurs only when a thick layer of the intermediate-wetting phase separates phases 1 and 3, as sketched in configuration 3 of Fig. 1 for a simple corner. In other words, for bulk phase 1 a 23 AM occurs only in combination with a 12 AM. In Section 4.1 we discuss the precise necessary criteria for the presence of a given AM in corners with straight walls.

[1] Notice that there is a typographical error in Eq. (18) of [7]: the third line of the equation should start with a minus sign, i.e., $-\{\sigma_{12} g^{(\alpha)}(r_{12}, \theta_{12}) + \cdots\}$.

For the 12 and 13 bulk phase combinations, Eq. (19) can be simplified to

$$-\sigma_{12} g(r_{12}, \theta_{12}) + \sum_{k=1}^{n} \sum_{ij=12,13,23} \sigma_{ij}\, g^{(k)}(r_{ij}, \theta_{ij}) \delta_{ij,a}^{(k)} - \sum_{k=1}^{n} \sigma_{23} g^{(k)}(r_{23}, \theta_{23}) \delta_{23,b}^{(k)} = 0, \tag{21a}$$

$$-\sigma_{13} g(r_{13}, \theta_{13}) + \sum_{k=1}^{n} \sum_{ij=12,13,23} \sigma_{ij}\, g^{(k)}(r_{ij}, \theta_{ij}) \delta_{ij,a}^{(k)} = 0, \tag{21b}$$

respectively. Taking the configuration of Fig. 2 as an example of a 12 displacement, we find for Eq. (21a) that in cross-section $a$, $\delta_{12,a}^{(k)} = 1$ and $\delta_{23,a}^{(k)} = 1$ in the lower right corner, while $\delta_{13,a}^{(k)} = 1$ in the lower left corner. Similarly, in cross-section $b$, $\delta_{23,b}^{(k)} = 1$ in all corners. Notice, that in the lower right corner the difference $\delta_{23,a}^{(k)} - \delta_{23,b}^{(k)}$ is equal to zero, as the same 23 AMs occur in both cross-sections.

Moreover, for the 12 displacement a special case arises when bulk phase 1 is completely surrounded by layers of the intermediate-wetting phase, such that 13 AMs are absent [7]. Then, only the difference $\delta_{12,a}^{(k)} - \delta_{12,b}^{(k)}$ in Eq. (19) is non-zero and Eq. (21a) depends on $r_{12}$ only. Similarly, for the 13 displacement in the absence of layers, only 13 AMs can be present and Eq. (21b) depends on $r_{13}$ only. In both special cases, as well as for the 23 displacement, where only 23 AMs can be present anyway, Eq. (19) reduces to the two-phase equation

$$-g(r_{ij}, \theta_{ij}) + \sum_{k=1}^{n} g^{(k)}(r_{ij}, \theta_{ij}) \delta_{ij,a}^{(k)} = 0 \tag{22}$$

for $ij = 12, 13, 23$.

Notice, that if no AMs are present Eq. (22) reduces further to

$$-g(r_{ij}, \theta_{ij}) = 0. \tag{23}$$

This equation can be used for example for a capillary of cylindrical cross-section with radius $r$. Using $A = \pi r^2$ and $L_s = 2\pi r$ in Eq. (18), we find

$$r_{ij} = \frac{r}{2\cos\theta_{ij}}. \tag{24}$$

Then, according to Eq. (10) the pressure difference $P_{ij}$, which we identify with the capillary entry pressure $P_{c,ij}$, obeys the traditional Young–Laplace equation $P_{c,ij} = 2\sigma_{ij}\cos\theta_{ij}/r$.

In Section 5, we will discuss examples of the above displacements for a specific cross-section. As indicated above the validity of some of these solutions also strongly depends on the presence of layers of the intermediate-wetting phase 2. In the next section we show how the existence of these layers follows from Eq. (19), when considering the 11 bulk phase combination. Since for the 33 bulk phase combination, no AMs can be present, Eq. (19) reduces to the

meaningless equation $0 = 0$. We comment on the 22 bulk phase combination at the end of Section 3.3, which may only lead to a rather trivial displacement.

In summary, non-trivial displacements arise from the 11, 12, 13 and 23 bulk phase combinations. The 11 combination leads to a criterion for the existence of phase 2 layers, the 12 and 13 combinations correspond in general to genuine three-phase displacements, but they may degenerate such that effectively two-phase displacement results, and the 23 combination always corresponds to a two-phase displacement.

### 3.3. Capillary entry of layers of the intermediate-wetting phase

For the 11 bulk phase combination, a non-trivial displacement exists associated with Eq. (19), which has not been identified in [7]. In this case a thick layer of phase 2 is present in cross-section $a$, surrounded by 12 and 23 AMs, while in cross-section $b$ only a 13 AM is present. Assuming that these layers occur independently in different corners or cavities, we consider this displacement separately in a given corner $k$. A section of a capillary through such a corner is sketched in Fig. 4. For the case of corners with straight walls, the respective corner cross-sections are shown in configurations 3 and 2 (with phases 1 and 3) of Fig. 1. For the remaining corners identical AMs are assumed in either cross-section.

Notice that in Fig. 4 the most general configuration is shown, where all three AMs are allowed to be present. For this displacement, we choose equal fluid distributions in cross-sections $a$ and $b$, except in corner $k$. Hence, in Eq. (19) the bulk phase term is absent and only in corner $k$ non-zero contributions arise, i.e., $\delta^{(k)}_{12,a} = 1$, $\delta^{(k)}_{23,a} = 1$ and $\delta^{(k)}_{13,b} = 1$, yielding

$$\sigma_{12} g^{(k)}(r_{12}, \theta_{12}) + \sigma_{23} g^{(k)}(r_{23}, \theta_{23}) - \sigma_{13} g^{(k)}(r_{13}, \theta_{13}) = 0. \tag{25}$$

In the derivation of Eq. (19) we have preserved the sign of the original energy variation $dF_T$ from Eq. (8). This energy variation is associated with a small displacement $dx$, which is taken positive when in the configuration of Fig. 4 the lengths of the 12 and 23 interfaces increase and the length of the 13 interface decreases. In other words, a positive value of $dx$ corresponds to (further) spreading of the phase 2 layer between phases 1 and 3 and a negative value of $dx$ corresponds to retraction of the phase 2 layer. Hence, if for some combination of radii, or equivalently phase pressures, the energy variation satisfies $dF_T > 0$, spreading of the phase 2 layer is unfavourable, and, vice versa, if $dF_T < 0$, spreading is favourable.

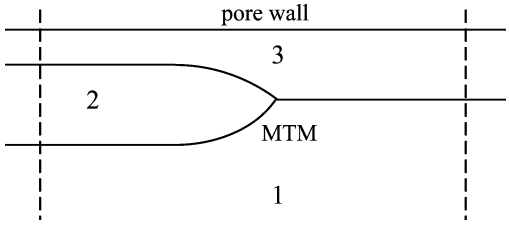


Fig. 4. Section through a corner along the length of a capillary where the MTM separates cross-sections with and without a layer of phase 2.

In Section 4.2 we show that for corners with straight walls as shown in Fig. 1, Eq. (25) can be worked out to find an explicit solution, which delineates the corresponding radii of curvature, i.e., pressure differences for which layers may or cannot exist. However, the free energy differential is not the only criterion for the existence of layers. Also geometrical criteria play a role, which have been derived for simple corners in [11,12].

**Remark.** For the 2 bulk phase combination we may consider similar to the spreading of a phase 2 layer, the spreading of a phase 3 wetting film in the corner or cavity of a capillary that is bulk filled with phase 2, respectively. Then, for one corner we find similar to Eq. (25)

$$g^{(k)}(r_{23}, \theta_{23}) = 0 \tag{26}$$

as only on one side of the MTM a single 23 AM is assumed to be present. It can be shown that for any corner geometry, Eq. (26) has the trivial solution $r_{23} = 0$ and that, based on the corresponding energy variation, the spreading of the wetting film is favourable for all radii $r_{23} > 0$. Consequently, if a 23 AM is allowed, the wetting phase will be present in the corner for all positive values of the pressure difference $P_{23}$, which we expect physically. Similarly, for the 11 bulk phase combination we may consider spreading of a phase 3 film in the corner.

## 4. Geometrical relations and conditions for the presence of interfaces and intermediate-wetting phase layers in polygonal cross-sections

### 4.1. Geometrical relations for capillaries with polygonal cross-section

For capillaries with polygonal cross-sections it is relatively easy to work out the geometrical functions needed in the derivation of capillary entry pressures and the criterion for existence of intermediate-wetting layers. Most important are the areas and lengths of contact, which are indicated in Fig. 3 for a simple corner with straight walls.

Following [7], we write

$$A^{(k)} = r^2 \left( \theta + \gamma^{(k)} - \frac{\pi}{2} + \cos\theta \left( \frac{\cos\theta}{\tan\gamma^{(k)}} - \sin\theta \right) \right), \tag{27a}$$

$$L_s^{(k)} = 2r \left( \frac{\cos\theta}{\tan\gamma^{(k)}} - \sin\theta \right), \tag{27b}$$

$$L_f^{(k)} = 2r \left( \frac{\pi}{2} - \theta - \gamma^{(k)} \right). \tag{27c}$$

Notice that for this corner geometry Eq. (18b) reduces to

$$g^{(k)}(r,\theta) = -\frac{A^{(k)}(r,\theta)}{r}. \tag{28}$$

Furthermore, similar to the function $f_T$ of [5], we introduce the function

$$h^{(k)}(\theta) = \theta + \gamma^{(k)} - \frac{\pi}{2} + \cos\theta\left(\frac{\cos\theta}{\tan\gamma^{(k)}} - \sin\theta\right), \tag{29}$$

which depends on $\theta$ only for a given corner $\alpha$, such that $A^{(k)}(r,\theta) = r^2 h^{(k)}(\theta)$.

The actual presence of an AM for a given fluid–fluid combination is determined by a simple geometrical criterion relating the contact angle of the interface to the corner half angle, i.e.,

$$\theta < \frac{\pi}{2} - \gamma^{(k)}. \tag{30}$$

Additionally, for the presence of two AMs in one corner surrounding an intermediate-wetting layer, as sketched in configuration 3 of Fig. 1, the necessary geometrical condition is [11,12]

$$\frac{r_{12}}{r_{23}} > \begin{cases} \frac{\cos(\theta_{23}+\gamma^{(k)})}{\cos(\theta_{12}+\gamma^{(k)})} & \text{if } \theta_{23} \leqslant \theta_{12}, \\ \frac{\cos\theta_{23}-\sin\gamma^{(k)}}{\cos\theta_{12}-\sin\gamma^{(k)}} & \text{if } \theta_{23} > \theta_{12}, \end{cases} \tag{31}$$

in terms of the associated radius of curvatures. In other words, if condition (30) is satisfied for the 12 and 23 AMs and additionally condition (31) applies, a layer of the intermediate-wetting phase 2 may arise. However, if condition (30) is also satisfied for the 13 AM in the same corner, the presence of a single 13 AM in that corner is an alternative configuration that cannot be ruled out by conditions (30) and (31) only. The sufficient condition for the existence of such a layer follows from Eq. (25), which we work out in the next section.

### 4.2. Existence of a layer of the intermediate-wetting phase

Equation (25) describing the displacement where phase 2 invades in the form of an intermediate-wetting layer can be worked out for a simple corner, using Eq. (28), as

$$-\sigma_{12}\frac{A_{12}^{(k)}}{r_{12}} - \sigma_{23}\frac{A_{23}^{(k)}}{r_{23}} + \sigma_{13}\frac{A_{13}^{(k)}}{r_{13}} = 0. \tag{32}$$

Then, using Eq. (20) for $r_{13}$ and Eq. (29) in Eq. (32) yields the quadratic equation for the ratio $r_{12}/r_{23}$,

$$\begin{aligned} &-\sigma_{12}\sigma_{23}h^{(k)}(\theta_{12})\left(\frac{r_{12}}{r_{23}}\right)^2 \\ &\quad + \left(\sigma_{13}^2 h^{(k)}(\theta_{13}) - \sigma_{12}^2 h^{(k)}(\theta_{12}) - \sigma_{23}^2 h^{(k)}(\theta_{23})\right)\frac{r_{12}}{r_{23}} \\ &\quad - \sigma_{12}\sigma_{23}h^{(k)}(\theta_{23}) = 0, \end{aligned} \tag{33}$$

which has the two solutions

$$\begin{aligned} &\left(\frac{r_{12}}{r_{23}}\right)_{\pm} \\ &\quad = \frac{\sigma_{13}^2 h^{(k)}(\theta_{13}) - \sigma_{12}^2 h^{(k)}(\theta_{12}) - \sigma_{23}^2 h^{(k)}(\theta_{23}) \pm \sqrt{D}}{2\sigma_{12}\sigma_{23}h^{(k)}(\theta_{12})}, \end{aligned} \tag{34}$$

identified by the sign before $\sqrt{D}$, if the discriminant

$$\begin{aligned} D = &\left(\sigma_{13}^2 h^{(k)}(\theta_{13}) - \sigma_{12}^2 h^{(k)}(\theta_{12}) - \sigma_{23}^2 h^{(k)}(\theta_{23})\right)^2 \\ &- 4\sigma_{12}^2\sigma_{23}^2 h^{(k)}(\theta_{12})h^{(k)}(\theta_{23}) \end{aligned} \tag{35}$$

is greater than or equal to zero. Obviously, if $D = 0$ the two solutions coincide and no solutions exist if $D < 0$.

Observe that Eq. (34) predicts combinations of the radii $r_{12}$ and $r_{23}$, hence using Eq. (20) also the radius $r_{13}$, at which phase 2 starts spreading (or retracting) between phases 1 and 3. However, because this is not a bulk displacement, we cannot identify one associated capillary entry pressure, as we would do for the other bulk displacements associated with Eq. (19). Instead, we find a combination of capillary pressures, say $P_{12}$ and $P_{23}$, at which the displacement of the phase 2 layer occurs.

Considering the sign of the left-hand side of Eq. (33), i.e., the sign of the associated energy variation $dF_T$, it is easy to show that $h^{(k)}(\theta) > 0$ if for a given AM condition (30) is satisfied. Therefore, if $D > 0$ and condition (30) is satisfied for all three AMs, the energy variation $dF_T$ is positive for $r_{12}/r_{23}$ lying between the two solutions (34) and negative elsewhere. Moreover, under these conditions both solutions are positive. Hence, in terms of the free energy variation, a layer of phase 2 can exist only if

$$\frac{r_{12}}{r_{23}} < \left(\frac{r_{12}}{r_{23}}\right)_{-} \quad \text{or} \quad \frac{r_{12}}{r_{23}} > \left(\frac{r_{12}}{r_{23}}\right)_{+}. \tag{36}$$

If $D < 0$ but condition (30) is still satisfied for all three AMs, no solutions of Eq. (33) exist and the left-hand side of the latter is negative for all $r_{12}/r_{23}$, i.e., the associated free energy is always decreasing. This means that in terms of free energy a layer of phase 2 can exist for any radius or pressure combination.

However, not only the free energy differential but also the geometrical condition (31) determines the actual existence of intermediate-wetting layers. A further complication of the existence criterion is that Eq. (25), as well as condition (31), degenerate if according to condition (30) one or more of the AMs cannot be present in the corner. We will deal with this complication below, when discussing the numerical examples in Section 5. However, if condition (30) is met for all 3 types of interfaces in a particular corner and $D > 0$, a thick layer of phase 2 exists if both conditions (31) and (36) are met. When $D < 0$ a thick layer of phase 2 exists, if only condition (31) is met.

It is worthwhile to mention that for most parameter combinations leading to $D > 0$ condition (31) includes $r_{12}/r_{23} > (r_{12}/r_{23})_+$ but excludes $r_{12}/r_{23} < (r_{12}/r_{23})_-$, such that

Table 1
Fluid–fluid parameters (interfacial tension ratio and contact angles) for determination of radii of curvatures for capillary entry pressures and for the presence of a phase 2 layer in the corner of a capillary. Furthermore, we list a characteristic feature for each case and indicate in which figure these cases are used

| Case | $\sigma_{12}/\sigma_{23}$ | $\theta_{23}$ | $\theta_{12}$ | $\theta_{13}$ | Comment |
|---|---|---|---|---|---|
| 1 | 0.2 | 0 | 0 | 0 | $D = 0$: one solution used in Fig. 9 |
| 2 | 0.3 | 0.5 | 0.813 | 0.444 | $D > 0$: general case used in Figs. 8 and 10 |
| 3 | 0.2 | 0.5 | 0 | 0.456 | $D < 0$: still condition (31) |
| 4 | 0.5 | 0 | 1.16 | 0 | 12 AM absent |
| 5 | 0.5 | 1.2 | 0.938 | 0.990 | 23 AM absent |
| 6 | 0.5 | 1.4 | 0.865 | 1.15 | 13 and 23 AMs absent |
| 7 | 0.3 | 1.0 | 0.733 | 0.881 | $D > 0$: general case used in Fig. 11 |

the condition $r_{12}/r_{23} > (r_{12}/r_{23})_+$ is sufficient. Situations where condition (31) does not exclude the latter involve fluid configurations where the distances between the involved fluid–fluid interfaces become very small and other forces that are not included in the present model, such as the disjoining pressure, start to play a major role.

Observe that spreading of the phase 2 layer may happen even if the spreading coefficient of phase 2, $C_{S,2} = \sigma_{13} - \sigma_{12} - \sigma_{23}$, is negative. The latter would prevent spreading of phase 2 in a free fluid situation [16], but in a capillary also fluid–solid interactions play a role, captured by $\theta_{ij}$ in conditions (30), (31) and (36), which lead to a more complicated criterion. On the other hand, if according to the spreading coefficient phase 2 spontaneously spreads between phases 1 and 3, the above criteria may prevent the existence of a thick layer of phase 2 for certain radius combinations. However, in these circumstances a molecularly thin film of phase 2 must exist between phases 1 and 3, but this phenomenon is not captured in our model, as we give only criteria for the existence of a thick layer.

In Appendix A we show that Eq. (33) can also be derived from the free energy balance for the spreading of a phase 2 layer, where the lengthening of the layer is balanced by the reduction of its thickness. This case was studied originally by Dong et al. [8] who came up with an equation for the radii of curvature that is eventually identical to Eq. (33), although they failed to find the explicit solution (34).

## 5. Numerical examples for a capillary with a cross-section in the shape of an isosceles triangle

To illustrate the impact of Eq. (19) we show a number of examples of calculation of the radii of curvature related to both piston-like displacements and to the presence of phase 2 layers in a single corner. For these calculations we fix the ratio of interfacial tension $\sigma_{13}/\sigma_{23} = 1.2$ and vary the ratio $\sigma_{12}/\sigma_{23}$ as well as the contact angles as shown in Table 1. Although the values of the contact angles are constrained by the Bartell–Osterhof equation (7) and an additional linear relationship between the $\cos\theta_{ij}$ as explained in [7,17], this does not restrict the generality of the method. Notice that cases 1 and 3 reflect the conditions of a spreading oil in a water-wet pore, since the spreading coefficient $C_{S,2} = \sigma_{13} - \sigma_{12} - \sigma_{23}$ yields $C_{S,2} = 0$, hence also $\theta_{12} = 0$. For the remaining cases $C_{S,2} < 0$ reflecting non-spreading conditions.

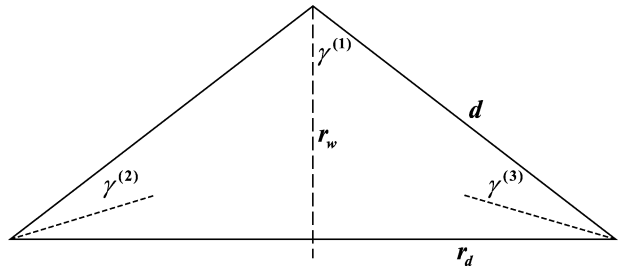


Fig. 5. Dimensions of isosceles triangle where $\gamma^{(2)} = \gamma^{(3)}$.

We take the isosceles triangle as an example of an angular pore cross-section with two unequal corner sizes, of which the geometry is sketched in Fig. 5. The area and perimeter of this triangle are $A = r_w r_d$ and $L_s = 2(d + r_d)$, whereas the inscribed radius is $r^{\text{in}} = r_d(d - r_d)/r_w$. The geometrical functions are given by Eqs. (27), with $\tan\gamma^{(1)} = r_d/r_w$ and $\tan\gamma^{(2)} = (d - r_d)/r_w$. Additionally, we define the aspect ratio $q = r_w/r_d$.

The snap-off radius $r_{ij}^{\max}$ for the phase combinations $ij = 12, 13, 23$ is found as

$$r_{ij}^{\max} = \begin{cases} \dfrac{d}{\sum_{k=1,2}\left(\frac{\cos\theta_{ij}}{\tan\gamma^{(k)}} - \sin\theta_{ij}\right)\delta_{ij}^{(k)}} & \text{if } \gamma^{(1)} \leqslant \gamma^{(2)}, \\ \dfrac{r_d}{\left(\frac{\cos\theta_{ij}}{\tan\gamma^{(2)}} - \sin\theta_{ij}\right)\delta_{ij}^{(2)}} & \text{if } \gamma^{(1)} > \gamma^{(2)}, \end{cases} \tag{37}$$

where $\delta_{ij}^{(k)}$ is used as $\delta_{ij,z}^{(k)}$ in Eq. (14b), but without reference to a specific side $z$. Beyond this radius the AMs from different corners meet and the corner phase snaps off the bulk phase [7]. Notice that $r_{ij}^{\max} = \infty$ if any of the denominators in Eq. (37) vanishes, i.e., when the corresponding AMs are absent, hence no snap-off will occur. A rather exceptional case, which we will not discuss any further, may arise when AMs of different types meet.

### 5.1. A layer of the intermediate-wetting phase in one corner

First, we examine the existence of thick layers of the intermediate-wetting phase for a single corner, as discussed in Section 4.2. For the half angle of the corner we take $\gamma^{(k)} = \pi/6$, which is the value for an equilateral triangle.

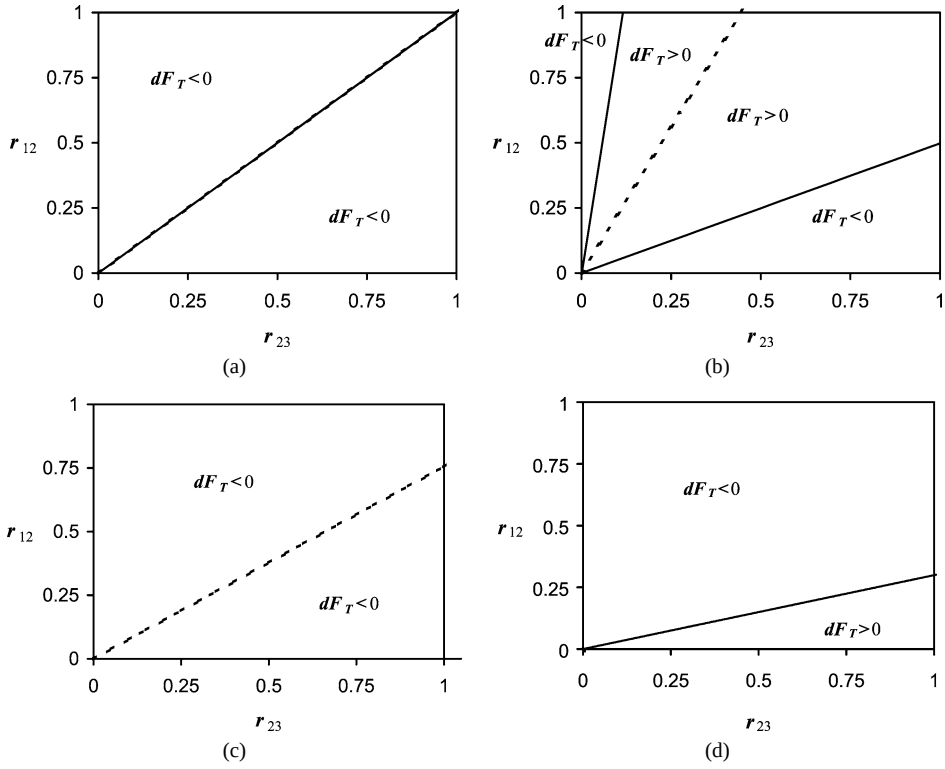


Fig. 6. Criteria for existence of a layer of the intermediate-wetting phase for (a) case 1, (b) case 2, (c) case 3, and (d) case 5 of Table 1, respectively. The solid lines are solutions of Eq. (34) and the dashed lines relate to condition (31). Layers can occur only for combinations of the AM radii of curvature $r_{12}$ and $r_{23}$, when $dF_T < 0$, as indicated, and condition (31) is satisfied, i.e., above the dashed lines.

Because we will connect the existence of layers with the capillary entry conditions for piston-like displacement of phases 1 and 2 in Section 5.2, we have chosen to plot the layer criteria in the $(r_{12}, r_{23})$ plane, as presented in Fig. 6.

The parameters of case 1 of Table 1 reflect a strongly water-wet corner with a spreading oil. Obviously, condition (30) is satisfied for all three AMs. Since $D = 0$, Eq. (33) has only one solution $r_{12}/r_{23} = 1$, which coincides with the criterion following from condition (31). Therefore, although we find $dF_T < 0$ on either side of the solutions as shown in Fig. 6a, a layer of phase 2 can exist only for $r_{12}/r_{23} > 1$.

Case 2 reflects a weakly water-wet corner with a non-spreading oil. Condition (30) is still satisfied for all three AMs, but in this case we find $D > 0$, such that Eq. (33) has the two solutions (34). Hence, two areas exist where $dF_T < 0$ and a layer may arise as shown in Fig. 6b, but condition (31) excludes the area below $(r_{12}/r_{23})_-$. Case 3 reflects a weakly water-wet corner with a spreading oil. Condition (30) is satisfied for all three AMs, but we find $D < 0$, such that Eq. (33) has no solutions. Therefore, we have $dF_T < 0$ for all positive values of $r_{12}$ and $r_{23}$, although condition (31) restricts the existence of a layer of phase 2 to the area above the criterion indicated in Fig. 6c.

The parameters of cases 4–6 correspond to situations in which one or more of the AMs cannot be present in the corner. Case 4 reflects a strongly water-wet corner with a non-spreading oil. Although $\theta_{13}$ and $\theta_{23}$ satisfy condition (30), this is not the case for $\theta_{12}$. Consequently, the 12 AM cannot be present in the corner, hence a layer of phase 2 cannot exist at all. On the other hand, case 5 reflects a very weakly water-wet pore with a non-spreading oil, such that $\theta_{23}$ does not satisfy condition (30). Since the remaining two contact angles still satisfy this condition, we may have a displacement as sketched in Fig. 7a, where phase 2 occupies the corner as if it were the wetting phase. Now Eq. (32) degenerates to

$$-\sigma_{12}\frac{A_{12}^{(k)}}{r_{12}} + \sigma_{13}\frac{A_{13}^{(k)}}{r_{13}} = 0, \tag{38}$$

yielding one solution for the ratio $r_{12}/r_{13}$. However, using relation (20), we may rewrite this solution in terms of $r_{12}$ and $r_{23}$, yielding

$$\frac{r_{12}}{r_{23}} = \frac{\sigma_{13}^2 h^{(k)}(\theta_{13}) - \sigma_{12}^2 h^{(k)}(\theta_{12})}{\sigma_{12}\sigma_{23} h^{(k)}(\theta_{12})}. \tag{39}$$

In Fig. 6d we have plotted this solution, where $dF_T < 0$ for $r_{12}/r_{23}$ above this value, as can be derived from the left-hand side of the reduced equation (33). Notice, that in this case condition (31) is not applicable, since the 23 AM is absent and the presence of a layer is purely restricted by the single solution of Eq. (33).

Finally, case 6 reflects a very weakly water-wet pore, where not only the 23 but also the 13 AM cannot be present. In this case we may have a displacement as sketched in Fig. 7b and the corresponding equation follows, similar to Eq. (26), as $g^{(k)}(r_{12}, \theta_{12}) = 0$. This leads to the single trivial

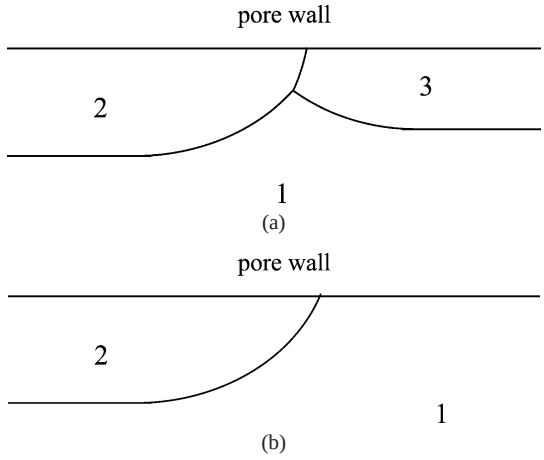


Fig. 7. Sections through a corner along the length of a capillary where the MTM separates cross-sections with and without a layer of phase 2, but (a) without a 23 AM and (b) without both a 13 and a 23 AM.

solution $r_{12} = 0$, while we find easily that $dF_T < 0$ for all $r_{12} > 0$. Hence, this type of layer will always exist, i.e., under the given circumstances phase 2 spreads unconditionally in the corner of the capillary in the presence of bulk phase 1.

### 5.2. Capillary entry conditions for the isosceles triangle

#### 5.2.1. Two-phase displacements

For the isosceles triangle the relevant two-phase solutions follow from Eq. (22), with $n = 3$ and $\delta_{ij,a}^{(k)} = 1$ in the corners where condition (30) for $\theta_{ij}$ is satisfied. Equation (22) can be written in quadratic form and solved explicitly for $r_{ij}$. For example, for the equilateral triangle where $\gamma^{(k)} = \pi/6$, we arrive at the well-known solutions [18,19]

$$r_{ij} = \begin{cases} \dfrac{r^{\text{in}}}{\cos\theta_{ij} \pm \sqrt{\frac{1}{\sqrt{3}}\left(\frac{\pi}{3} - \theta_{ij} + \sin\theta_{ij}\cos\theta_{ij}\right)}} & \text{if } \theta_{ij} < \frac{\pi}{3}, \\ \dfrac{r^{\text{in}}}{2\cos\theta_{ij}} & \text{if } \theta_{ij} \geqslant \frac{\pi}{3}. \end{cases} \tag{40}$$

For $\theta_{ij} < \pi/3$ the solution with the $-$ sign in the denominator is normally discarded, because for this solution the radius is larger than the snap-off radius, i.e., $r_{ij} > r_{ij}^{\max}$, where $r_{ij}^{\max}$ is defined by Eq. (37). For $\theta_{ij} > \pi/3$ the solution follows from Eq. (23), and it is the same as for a circular cross-section (24) with $r^{\text{in}} = r$.

As discussed in Section 3.2, in three-phase flow there are essentially three genuine three-phase displacements. First, there is the layer displacement. Second, there is the bulk phase displacement of phases 1 and 2 with phase 3 in the corners, such that phases 1 and 3 share an AM in at least one corner. Third, there is the bulk phase displacement of phases 1 and 3 where phases 2 and 3 share an AM in at least one corner. In the next subsections, we discuss examples of the latter two displacements and combine them with the criteria for the existence of layers.

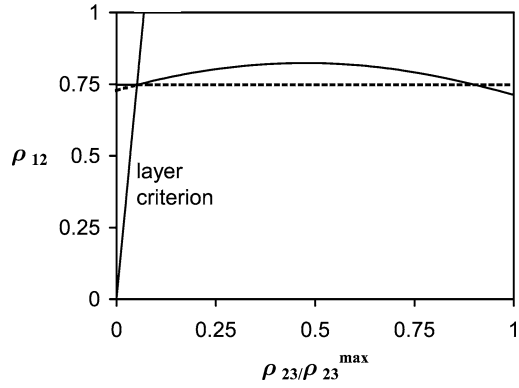


Fig. 8. Varying and constant dimensionless solutions for the radius of curvature $\rho_{12}$, corresponding to the capillary entry pressures for piston-like displacement of phases 1 and 2 in an equilateral triangle, as a function of the normalised dimensionless radius $\rho_{23}$, which represents the wetting phase 3 pressure, for the parameters of case 2. Additionally, the sloped line is the relevant solution for layer displacements separating the ranges of validity of the constant and varying solutions, which are indicated as solid curves when valid and as dashed curves when not valid.

#### 5.2.2. Bulk phase displacement of phases 1 and 2 affected by phase 3

For the three-phase displacement of phases 1 and 2, where 13 AMs are present in every corner on one side of the MTM and 23 AMs are present in every corner on the opposite side of the MTM, Eq. (21a) applies as

$$-\sigma_{12} g(r_{12}, \theta_{12}) + \sigma_{13} \sum_{k=1}^{3} g^{(k)}(r_{13}, \theta_{13}) - \sigma_{23} \sum_{k=1}^{3} g^{(k)}(r_{23}, \theta_{23}) = 0. \tag{41}$$

Using relation (20), we may write Eq. (41) as a functional relation between any two of the three radii of curvature. Using also Eq. (7), we choose to write Eq. (41) as a relation between the radii $r_{13}$ and $r_{23}$, i.e.,

$$\sigma_{13}\left\{-g(r_{13}, \theta_{13}) + \sum_{k=1}^{3} g^{(k)}(r_{13}, \theta_{13})\right\} - \sigma_{23}\left\{-g(r_{23}, \theta_{23}) + \sum_{k=1}^{3} g^{(k)}(r_{23}, \theta_{23})\right\} = 0, \tag{42}$$

where the first two terms and the last two terms have the same form as the left-hand side of the two-phase equation (22). Hence, Eq. (42) can be written as a quadratic equation for the radius $r_{13}$, which depends on the value of $r_{23}$. Consequently, for those values of $r_{23}$ for which the discriminant of this equation in terms of $r_{13}$ is positive, Eq. (42) has two solutions. Using again relation (20), we transform these into two solutions for $r_{12}$, which vary with the radius $r_{23}$.

In Appendix B we discuss the physical constraints that leave us with only one of these solutions for $r_{12}$ for a limited range of $r_{23}$ values, which is plotted in Fig. 8 for the parameters of case 2 in Table 1 in case of an equilateral triangle.

These constraints are, basically, that the radii of curvature at the relevant AMs and the MTM are positive and that the radii at the AMs are smaller than the corresponding snap-off radii $r_{ij}^{\max}$, as defined in Eq. (37). In Fig. 8 we have introduced the dimensionless radii $\rho = r/r^{\text{in}}$ and we have normalised the $\rho_{23}$ values by the snap-off value $\rho_{23}^{\max}$ for comparison with other cases. The radius $\rho_{23}$ represents the value of the pressure in the wetting phase 3, which does affect the value of the radius $\rho_{12}$ reflecting the 12 capillary entry condition.

In Fig. 8 we have added, in dimensionless form, the remaining relevant solution $(\rho_{12}/\rho_{23})_+$ for layer displacements following from Eq. (34). As explained for Fig. 6b, layers of phase 2 are absent below $(\rho_{12}/\rho_{23})_+$, hence the varying solution of Eq. (41) is valid on this side of the $(\rho_{12}, \rho_{23})$ plane only. On the other hand, when layers are present in all corners, the constant solution for $\rho_{12}$ following from Eq. (40), which is also presented in Fig. 8, is found. Obviously, this solution is valid only when layers of phase 2 are present, i.e., above $(\rho_{12}/\rho_{23})_+$.

Observe that $(\rho_{12}/\rho_{23})_+$ and the constant and varying solutions for $\rho_{12}$ intersect at exactly the same point. This can easily be explained from the underlying equations (25), (24) and (41), respectively, and it confirms that $(\rho_{12}/\rho_{23})_+$ provides indeed the necessary and sufficient condition for distinguishing between the constant and the varying solutions. Notice that these solutions intersect again, which corresponds to the intersection with the discarded solution $(\rho_{12}/\rho_{23})_-$ of Eq. (34).

A final restriction on the validity of the above solutions arises in an interconnected network of pores when phase 3 is available as bulk phase in a capillary adjacent to the considered capillary. Then, for sufficiently large values of the phase 3 pressure, this phase may displace the bulk phase that is present in the capillary, before the targeted displacement between phases 1 and 2 can occur. For example, if phase 2 is present in the capillary and in an adjacent capillary $\rho_{23}$ exceeds the two-phase value for 23 displacement following from Eq. (40), phase 3 will displace phase 2 before phase 1. For the parameters of case 2, the value of the two-phase displacement radius $\rho_{23}$ is 0.615, i.e., 0.370 when normalised.

### 5.2.3. *Bulk phase displacement of phases 1 and 3 affected by phase 2*

For the three-phase displacement of phases 1 and 3, where 12 and 23 AMs are present in every corner to form layers of phase 2 on the side of the MTM where phase 1 is present, Eq. (21b) reduces to

$$-\sigma_{13} g(r_{13}, \theta_{13}) + \sigma_{12} \sum_{k=1}^{3} g^{(k)}(r_{12}, \theta_{12}) + \sigma_{23} \sum_{k=1}^{3} g^{(k)}(r_{23}, \theta_{23}) = 0. \tag{43}$$

Using relations (7) and (20), we choose to write Eq. (43) as a relation between the radii $r_{12}$ and $r_{23}$ similar to Eq. (42).

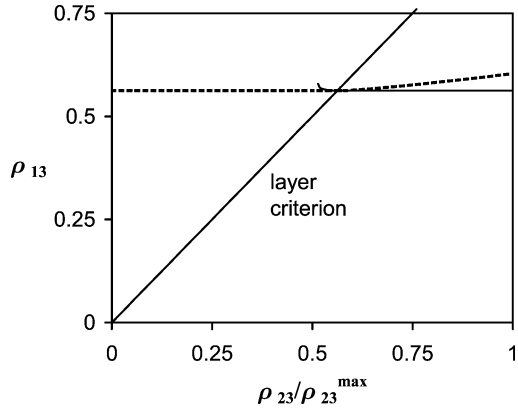


Fig. 9. Varying and constant dimensionless solutions for the radius of curvature $\rho_{13}$, corresponding to the capillary entry pressures for piston-like displacement of phases 1 and 3 in an equilateral triangle, as a function of the normalised dimensionless radius $\rho_{23}$, which represents the intermediate-wetting phase 2 pressure, for the parameters of case 1. Additionally, the sloped line is the relevant solution for layer displacements separating the ranges of validity of the constant and varying solutions, which are indicated as solid curves when valid and as dashed curves when not valid.

As for the 12 displacement, discussed in Section 5.2.2, we indicate in Appendix B the physical constraints that leave us with one solution for $r_{13}$ for a limited range of $r_{23}$ values, which is plotted in Fig. 9 for the parameters of case 1 in Table 1 in case of an equilateral triangle.

In this case the dimensionless radius $\rho_{23}$ represents the value of the pressure in the intermediate-wetting phase 2, which does affect the value of the radius $\rho_{13}$, reflecting the 13 capillary entry condition. In Fig. 9 we have added the remaining relevant solution for layer displacements following from Eq. (34) as $(\rho_{13}/\rho_{23})_+$. Layers of phase 2 are present for values of $(\rho_{13}, \rho_{23})$ above $(\rho_{13}/\rho_{23})_+$, hence the solution of Eq. (43) is valid on this side of the plane only. On the other hand, when layers of phase 2 separating phases 1 and 3 are absent in all corners, the constant solution for $\rho_{13}$ following from Eq. (40), which is also presented in Fig. 9, is found. This solution can only be valid below $(\rho_{13}/\rho_{23})_+$. Again $(\rho_{13}/\rho_{23})_+$ and the constant and varying solutions for $\rho_{13}$ intersect at exactly the same point.

From Fig. 9 it is clear that the possible range of validity of the varying solution above $(\rho_{13}/\rho_{23})_+$ is very small and it is very close to the constant solution. For most parameter combinations we find that the impact of a possible varying solution for $\rho_{13}$ is very small and we will not discuss this displacement any further. The alternative to the varying solution above $(\rho_{13}/\rho_{23})_+$ would be the constant solution, which occurs when no layers of phase 2 are present. But in a three-phase system where phase 2 is sufficiently available, layers must be present, hence the constant solution will not be found either, as indicated in Fig. 9. In this case, phase 2 in the layer will snap off bulk phase 1, before the intended 13 displacement occurs. However, if phase 2 is not available to the considered capillary, which is well possible in an interconnected pore network, the constant solution becomes possible again, although it relates now to a two-phase dis-

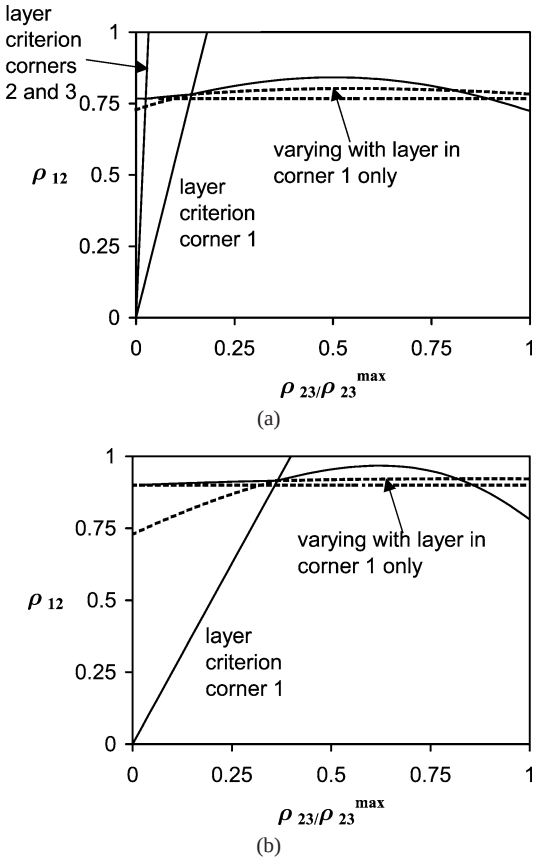


Fig. 10. Solutions for the radius of curvature $\rho_{12}$, corresponding to the capillary entry pressures for piston-like displacement of phases 1 and 2 in an isosceles triangle with (a) aspect ratio $q = 3$ and (b) aspect ratio $q = 10$, for the parameters of case 2, as a function of the normalised dimensionless radius $\rho_{23}$. The sloped lines indicate the layer criteria separating the ranges of validity of the various solutions, which are drawn as solid curves when valid and as dashed curves when not valid.

placement in a (locally) two-phase system. We will work out the various displacements for limited phase availability in more detail in a future paper.

### 5.2.4. *Displacement of phases 1 and 2 for an isosceles triangle of varying aspect ratio*

In Fig. 8 we have connected the criterion for existence of a phase 2 layer with the entry conditions for displacement of phases 1 and 2 in a capillary of equilateral triangular cross-section. Here, we consider the entry conditions for the more general geometry of an isosceles triangle with varying aspect ratio $q$ for the parameters of case 2 in Table 1, as sketched in Fig. 5. In the general isosceles triangle two differently sized corners arise, each of which has a different criterion for the existence of layers of phase 2. We choose to vary the aspect ratio such that the top corner 1 is always smaller than the base corners 2 and 3.

In Fig. 10 we have plotted the capillary entry conditions for two different aspect ratios of the triangle for the parameters of case 2 in Table 1. For aspect ratio $q = 3$ all three AMs can be present according to condition (30) in both the top corner and the base corners of the triangle. In Fig. 10a we find two different layer criteria, which indicate that between these two criteria a regime exists where a phase 2 layer can be present in one corner only, in this case the smaller top corner 1. Notice that each of these criteria follow from Eq. (34) as $(r_{12}/r_{23})_+$ for the respective corners, which in turn satisfy condition (31). Because there are criteria for two corner sizes, we must not only consider the constant solution for layers in all corners, following from Eq. (22), and the varying solution for no layers, following from Eq. (41), but also a varying solution when a layer of phase 2 is present in corner 1 only. In the latter case Eq. (21a) reduces to

$$-\sigma_{12}g(r_{12},\theta_{12}) + \sigma_{13}\sum_{k=2,3} g^{(k)}(r_{13},\theta_{13}) + \sigma_{12}g^{(1)}(r_{12},\theta_{12}) - \sigma_{23}\sum_{k=2,3} g^{(k)}(r_{23},\theta_{23}) = 0, \qquad (44)$$

similar to that for a pore of rhomboidal cross-section [7]. Equation (44) cannot be solved analytically, therefore we have used a Newton–Raphson method to find the relation between $r_{12}$ and $r_{23}$. In Fig. 10a we find that the constant solution and the solution of Eq. (44) intersect in one point with the layer criterion for corners 2 and 3. Furthermore, the two varying solutions intersect in one point with the layer criterion for corner 1. This is consistent, since the layer criterion for corners 2 and 3 separates the regimes where the constant solution and the solution for one layer are valid. Similarly, the two varying solutions connect continuously at the criterion for corner 1. Notice that for this value of the aspect ratio the three solutions can be well distinguished from each other.

For each of the three solutions we have checked that the involved AM radii of curvature do not lead to snap-off of one of the phases. For the 23 radius this is simply represented in Fig. 10a, since we have plotted the solution for $\rho_{23} < \rho_{23}^{\max}$ only. Notice that this condition is relevant for the solution without layers only, as only the range of this solution extends to $\rho_{23} = \rho_{23}^{\max}$. A similar argument applies to snap-off of the 13 AMs, which occur only in the configurations related to the two varying solutions. For the range of values $0 < \rho_{23} < \rho_{23}^{\max}$ the $\rho_{13}$ associated with these solutions is always well below $\rho_{13}^{\max}$. Similarly, the 12 AMs occurring for the constant solution and the solution of Eq. (44) satisfy $\rho_{12} < \rho_{12}^{\max}$.

In Fig. 10b we have plotted the possible solutions for aspect ratio $q = 10$. In this case all three AMs can still be present in all corners of the triangle according to condition (30). However, the layer criterion for corners 2 and 3 has become indistinguishable from the vertical axis. This already approximates the situation in which $\theta_{12}$ does not satisfy condition (30) in corners 2 and 3, which happens beyond $q = 17.9$, such that a layer cannot be present in these corners. We find again two varying solutions of which one corresponds to the presence of a phase 2 layer in corner 1 only, which is calculated from Eq. (44). This solution is valid for a significant regime above the remaining layer criterion, although it is not very different from the constant solution. On

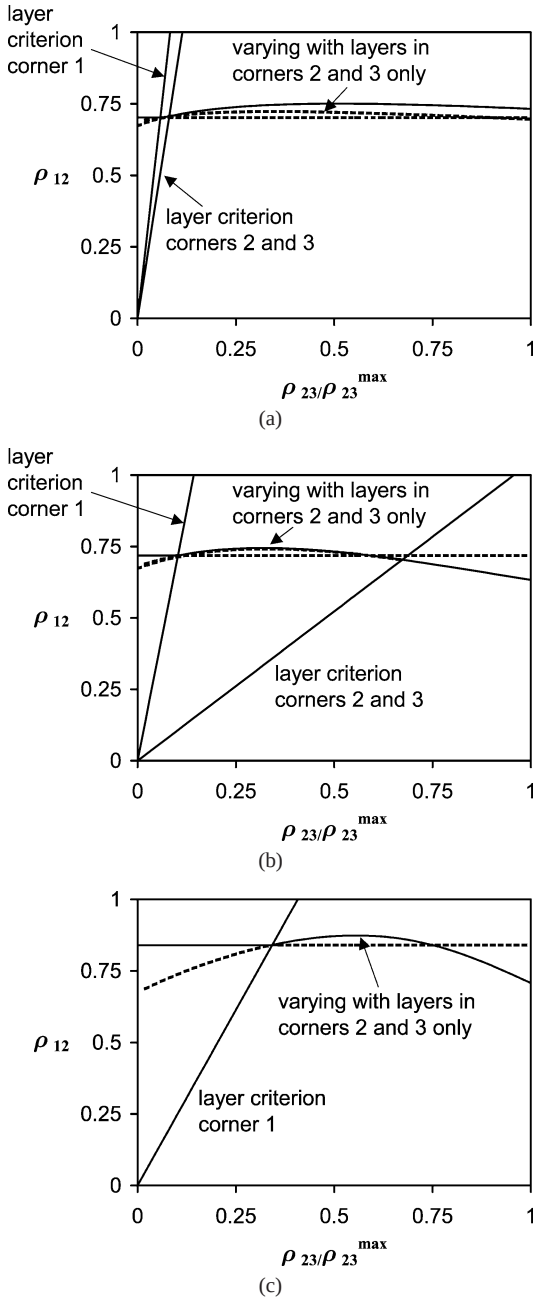


Fig. 11. Solutions for the radius of curvature $\rho_{12}$, corresponding to the capillary entry pressures for piston-like displacement of phases 1 and 2 in an isosceles triangle with (a) aspect ratio $q = 2$, (b) aspect ratio $q = 3$ and (c) aspect ratio $q = 10$, for the parameters of case 7, as a function of the normalised dimensionless radius $\rho_{23}$. The sloped lines indicate the layer criteria separating the ranges of validity of the various solutions, which are drawn as solid curves when valid and as dashed curves when not valid.

the other hand, the solution corresponding to the absence of layers in all corners varies significantly with the radius $\rho_{23}$.

In Fig. 11 we present also the entry conditions for displacement of phases 1 and 2 in a capillary of which the cross-section is an isosceles triangle, as sketched in Fig. 5, but now for the parameters of case 7 in Table 1. The main difference with case 2 is that for case 7, $\theta_{13}$ and $\theta_{23}$ are significantly larger, which reflects a more weakly water-wet capillary. This leads to an important difference in the layer criteria. It follows easily from Eq. (34) that for case 2 the relevant solution $(r_{12}/r_{23})_+$ is larger for corner 1 than for corners 2 and 3, whereas for case 7 it is the other way around. This means that for case 7 a regime exists where layers can be present in the larger corners 2 and 3 but not in the smaller top corner 1. For this case again a different varying solution is found, satisfying the equation

$$-\sigma_{12}g(r_{12},\theta_{12}) + \sigma_{13}g^{(1)}(r_{13},\theta_{13}) + \sigma_{12}\sum_{k=2,3} g^{(k)}(r_{12},\theta_{12}) - \sigma_{23}g^{(1)}(r_{23},\theta_{23}) = 0, \quad (45)$$

provided that the three AMs satisfy condition (30) in all corners, which is the case for aspect ratio $q = 2$.

The solution of Eq. (45) together with the usual constant and varying solutions are plotted in Fig. 11a. For this aspect ratio the two layer criteria are close together, because the geometry of the triangle is still close to equilateral, hence the range of validity of the solution of Eq. (45) is small. Furthermore, the latter solution is close to the constant solution. Although not well visible, we find consistently that the two varying solutions intersect in one point with the layer criterion for corners 2 and 3.

For aspect ratio $q = 3$ the 23 AM can no longer be present in corners 2 and 3. Therefore, possible layers in these corners are of the type sketched in Fig. 7a to the left of the MTM, where phase 3 is absent from the corner. The corresponding criterion is discussed in Section 5.1 related to case 5. Because the 23 AMs cannot be present in corners 2 and 3, Eq. (41) for the case without layers reduces to

$$-\sigma_{12}g(r_{12},\theta_{12}) + \sigma_{13}\sum_{k=1}^{3} g^{(k)}(r_{13},\theta_{13}) - \sigma_{23}g^{(1)}(r_{23},\theta_{23}) = 0. \quad (46)$$

Notice that Eqs. (22) and (45) for the case with layers in corners 2 and 3 remain the same, as these do not involve the 23 AMs in these corners. The solutions of Eqs. (22), (45) and (46) are plotted in Fig. 11b. For this aspect ratio the two layer criteria are far apart, hence the range of validity of the solution of Eq. (45) is significant. In several ways the entry conditions for this case vary opposite to those for case 2, presented in Fig. 10. For the larger aspect ratio the varying solution for layers in corners 2 and 3 only approaches the remaining varying solution, rather than the constant solution, and the range of validity of the constant solution has increased.

For aspect ratio $q = 10$ additionally the 13 AM can no longer be present in corners 2 and 3. As discussed in Section 5.1 for case 6 in these corners layers of phase 2, in the sense of Fig. 7b, are present unconditionally, as the corresponding layer criterion disappears. Hence, only the constant solution following from Eq. (22) remains and the varying solution following from Eq. (45) corresponding to layers in corners 2 and 3 only. We have plotted these solutions in

Fig. 11c, together with the remaining layer criterion for corner 1, as the criterion for corners 2 and 3 coincides with $\rho_{12} = 0$. There exists a large regime in which the constant solution is valid, while the deviation of the varying solution in the remaining regime is significant as a result of the large aspect ratio.

The above leads to the interesting conclusion that in a more weakly water-wet capillary, i.e., when $\theta_{23}$ is relatively large, the potential for layer spreading is greater in the larger than in the smaller corners, while in a more strongly water-wet corner, when $\theta_{23}$ is relatively small, the opposite is true. This is consistent with cases 5 and 6 discussed in Section 5.1, where $\theta_{23}$ is so large that the 23 AM cannot be present in the corners, which may even lead to spontaneous spreading of phase 2, irrespective of the phase 3 pressure.

## 6. Summary and conclusions

We have derived the free energy balance for all possible equilibrium configurations of two and three phases in a straight capillary of arbitrary cross-section. This balance has been reformulated into a general equation (19) to find the effective radii of curvatures or, equivalently, the capillary entry pressures related to piston-like displacements of two bulk phases, where also a third phase may be present. Moreover, the general equation successfully applies to the spreading between the wetting and the non-wetting phase of a thick layer of the intermediate-wetting phase in a corner or cavity of the capillary. When treating this spreading behaviour as a capillary displacement, the corresponding radii of curvature can be found, similar to those related to the piston-like displacements. Furthermore, using the energy balance all combinations of radii of curvatures, i.e., phase pressure combinations, can be determined for which such a layer exists. For a number of combinations of interfacial tensions and contact angles, illustrating all the different relevant situations, we have calculated the criteria for spreading of a layer in the corner of a capillary with polygonal cross-section. As shown in [7], the presence or absence of layers in the corner leads to different entry conditions for bulk–bulk displacements. Therefore, we have additionally calculated the capillary entry pressures for piston-like displacement in a capillary with a cross-section in the shape of an isosceles triangle of varying corner sizes to illustrate how the layer criteria can distinguish between the possible entry pressures.

Conclusions are as follows:

(i) The free energy balance for three phases in a capillary rigorously leads to the equation derived in [7] for the capillary entry pressures related to any piston-like displacement of two bulk phases in the presence of the remaining third phase, which actually applies in a straight capillary of any arbitrary cross-section. This equation additionally provides the phase pressure differences at which a layer of the intermediate-wetting phase will spread between the remaining two phases in the corners of a capillary.

(ii) The formulation of the general equation (19) shows that all possible displacements can be classified according to the combination of bulk phases on either side of the main terminal meniscus (MTM). Combination of different bulk phases corresponds to piston-like displacement and combination of identical bulk phases corresponds to spreading of layers and films in corners.

(iii) When complemented with the necessary geometric condition for the existence of layers [11,12], the presently derived criterion uniquely determines the presence of layers of the intermediate-wetting phase in most relevant cases.

(iv) Because the capillary entry conditions and the layer criterion are derived from the same free energy balance, the different possible entry conditions for a given piston-like displacement carry over into each other continuously at the pressure combination corresponding to the relevant layer criterion.

(v) A particular case of layer spreading occurs when the wetting phase cannot be present in the corner. In this case, the intermediate-wetting phase can spontaneously spread between the non-wetting phase and the solid. This is consistent with the observation that in a more weakly wetted capillary the potential for layer spreading is greater in the larger than in the smaller corners, whereas the opposite is true for more strongly wetted capillaries.

(vi) When layers of the intermediate-wetting phase entirely separate the wetting and the non-wetting phases in the cross-section of a capillary, the capillary entry pressure for piston-like displacement of the non-wetting and intermediate-wetting phases does not depend on the pressure of the wetting phase. However, in many cases the pressure combinations for which layers occur in all corners is very limited and capillary entry pressures arise, which may vary significantly with the wetting film pressure.

## Acknowledgments

The authors are grateful to A. Danesh for his helpful comments. M.I.J. van Dijke and K.S. Sorbie would like to thank the following members of the Heriot–Watt WAG Consortium for supporting this research: The UK Department of Trade and Industry, BP, Shell, PDVSA, BHP, Total, Norsk Hydro and Statoil.

## Appendix A. Review of analysis by Dong et al. [8]

Dong et al. analysed the spreading of the intermediate-wetting phase 2 between the non-wetting and the wetting

phases, 1 and 3, respectively, through analysis of the associated changes in surface free energy. They considered a water-wet system with oil as the intermediate-wetting phase and gas as the non-wetting phase, but it is clear that the analysis is applicable to any system of three fluid phases. However, contrary to the present analysis, Dong et al. considered also volume changes in the transversal direction, although assuming that these changes did not affect the phase pressures. They obtained an algebraic relation between the radii of curvature $r_{12}$ and $r_{23}$ constituting the critical thickness at which the layer spreads, which they solved numerically. Below we review their analysis and show that their expression for the variation of surface free energy is exactly the same as our equation for the total variation of free energy (32). Hence, their equation for the radii of curvature at critical thickness is the same as ours and their equation can also be solved analytically.

In Fig. 12a we show the change of contours of the layer, when phase 2 spreads out slightly between phases 1 and 3, by a distance $dx$ in the direction along the length of the capillary. As a result the 12 and 23 contacts surrounding the layer change, but the 13 contact is untouched. During this displacement volume of all phases is conserved, i.e., $dV_1 = dV_2 = dV_3 = 0$, hence from the geometry of Fig. 12 we obtain

$$dV_1 = -x\,dA_{12}^{(k)} - \left(A_{12}^{(k)} - A_{13}^{(k)}\right)dx = 0, \tag{A.1a}$$

$$dV_2 = x\,d\left(A_{12}^{(k)} - A_{23}^{(k)}\right) + \left(A_{12}^{(k)} - A_{23}^{(k)}\right)dx = 0, \tag{A.1b}$$

where the cross-sectional areas $A_{ij}^{(k)}$ are defined in Fig. 3 and shown in Fig. 12b with the area variations resulting from the displacement. For symmetry reasons we consider only one half of the layer, which has finite length $x$.

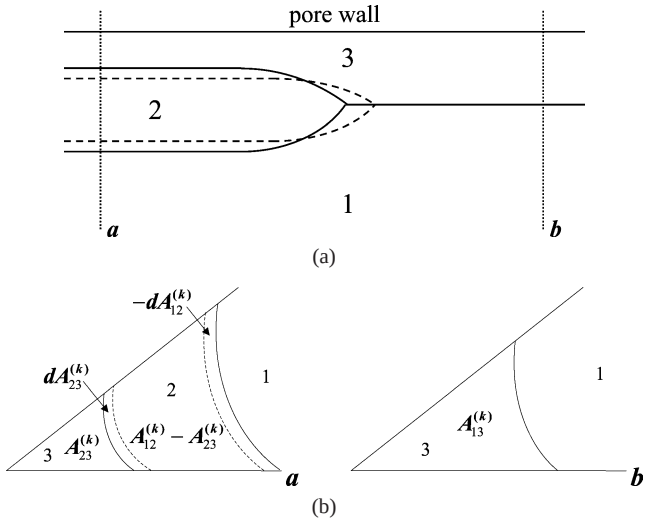


Fig. 12. (a) Section through a corner along the length of a capillary containing a layer of phase 2 separating phases 1 and 3. (b) Cross-sections of this corner. The dashed curves indicate the contour changes after slight spreading of the layer and in (b) the accompanying changes in cross-sectional areas are shown.

To find a relation between the various radii of curvature for the configuration at thermodynamic equilibrium, we apply again the energy balance (4). For the current small displacement the area variations of the contact surfaces are given by

$$dA_{12} = x\,dL_{f,12}^{(k)} + L_{f,12}^{(k)}\,dx, \tag{A.2a}$$

$$dA_{13} = -L_{f,13}^{(k)}\,dx, \tag{A.2b}$$

$$dA_{23} = x\,dL_{f,23}^{(k)} + L_{f,23}^{(k)}\,dx, \tag{A.2c}$$

$$dA_{1s} = -x\,dL_{s,12}^{(k)} - \left(L_{s,12}^{(k)} - L_{s,13}^{(k)}\right)dx, \tag{A.2d}$$

$$dA_{2s} = x\,d\left(L_{s,12}^{(k)} - L_{s,23}^{(k)}\right) + \left(L_{s,12}^{(k)} - L_{s,23}^{(k)}\right)dx. \tag{A.2e}$$

Hence, when also using relation (7), Eq. (4) reduces to

$$\begin{aligned}
&\sigma_{12}x\,d\left(L_{f,12}^{(k)} - \cos\theta_{12}L_{s,12}^{(k)}\right)\\
&\quad+\sigma_{12}\left(L_{f,12}^{(k)} - \cos\theta_{12}L_{s,12}^{(k)}\right)dx\\
&\quad-\sigma_{13}\left(L_{f,13}^{(k)} - \cos\theta_{13}L_{s,13}^{(k)}\right)dx\\
&\quad+\sigma_{23}x\,d\left(L_{f,23}^{(k)} - \cos\theta_{23}L_{s,23}^{(k)}\right)\\
&\quad+\sigma_{23}\left(L_{f,23}^{(k)} - \cos\theta_{23}L_{s,23}^{(k)}\right)dx = 0.
\end{aligned} \tag{A.3}$$

From Eqs. (27) we derive the relations between the lengths and areas of a phase occupying a corner and between their derivatives as

$$\begin{aligned}
&L_f^{(k)} - \cos\theta\cdot L_s^{(k)} = -\frac{2A^{(k)}}{r},\\
&d\left(L_f^{(k)} - \cos\theta\cdot L_s^{(k)}\right) = -\frac{dA^{(k)}}{r},
\end{aligned} \tag{A.4}$$

which transform Eq. (A.3) into

$$\begin{aligned}
&-\sigma_{12}x\frac{dA_{12}^{(k)}}{r_{12}} - 2\sigma_{12}\frac{A_{12}^{(k)}}{r_{12}}dx + 2\sigma_{13}\frac{A_{13}^{(k)}}{r_{13}}dx\\
&\quad-\sigma_{23}x\frac{dA_{23}^{(k)}}{r_{23}} - 2\sigma_{23}\frac{A_{23}^{(k)}}{r_{23}}dx = 0.
\end{aligned} \tag{A.5}$$

Application of the volume balances (A.1) to Eq. (A.5) and taking out $dx$ yields

$$-\sigma_{12}\frac{A_{12}^{(k)}}{r_{12}} + \sigma_{13}\frac{A_{13}^{(k)}}{r_{13}} - \sigma_{23}\frac{A_{23}^{(k)}}{r_{23}} = 0, \tag{A.6}$$

which is exactly the same as Eq. (32). We have already shown that an analytical solution of this equation can be found in terms of the ratio $r_{12}/r_{23}$ of the radii of curvature for the fluid–fluid surfaces surrounding the layer of phase 2. These radii of curvature can be used to find the critical thickness introduced by Dong et al. and it can be shown that our analytical results are the same as their numerical findings.

Interestingly, the various assumptions regarding the volume variations do not affect the resulting equation. That is, Dong et al. considered changes in width of the phase distributions to be volume balanced by changes in length, for which they had to assume explicitly that the phase pressures were constant. In the present analysis we assume variation in

the length of the distribution only, allowing a slight change of phase volumes.

## Appendix B. Constraints on the varying solutions for the radii of curvature related to three-phase piston-like displacements

For the three-phase displacement of phases 1 and 2 discussed in Section 5.2.2, where 13 AMs are present in every corner on one side of the MTM and 23 AMs are present in every corner on the other side of the MTM, Eq. (41) yields a relation between the radii $r_{12}$ and $r_{23}$. For displacement in an equilateral triangle this relation is plotted in Fig. 13a for the parameters of case 2 of Table 1. We observe that for most values of $r_{23}$, there exist two distinct solutions for $r_{12}$, except for a small range of negative $r_{23}$ values. However, we will discard most of the radius combinations as non-physical, a procedure for which we have to look carefully at the geometry of the corresponding interfaces.

During the considered 12 capillary displacement there are 13 and 23 AMs present in the corners. For these AMs we consider only positive values of the radii of curvature $r_{13}$ and $r_{23}$, as may be expected for realistic displacements in uniformly wetted pores in the absence of contact angle hysteresis [19]. Notice that $r_{13}$ is not directly represented in Fig. 13a, but using relation (20) we find the straight line in the $(r_{12}, r_{23})$ plane where $r_{13}$ changes sign, such that $r_{13} > 0$ above this line. Based on this criterion all radius combinations in the first quadrant of the $(r_{12}, r_{23})$ plane are allowed. The next restriction is that both $r_{13}$ and $r_{23}$ should be below their respective snap-off values, given by Eq. (37). For the parameters of case 2 we find $r_{13}^{\max} = 1.53$ and $r_{23}^{\max} = 1.66$, where the former translates into values of $r_{12}$, such that also the top curve in the first quadrant of Fig. 13a must be discarded. Using the described constraints, the remaining single valued part of the relation between $r_{12}$ and $r_{23}$ is shown in Fig. 8.

For the three-phase displacement of phases 1 and 3 discussed in Section 5.2.3, where 12 and 23 AMs are present in every corner on the side of the MTM where phase 1 is present, Eq. (43) yields eventually a relation between the radii $r_{13}$ and $r_{23}$. For displacement in an equilateral triangle this relation is plotted in Fig. 13b for the parameters of case 1 of Table 1. Again, we consider only positive values of the AM radii $r_{12}$ and $r_{23}$. From relation (20) we find the straight line in the $(r_{13}, r_{23})$ plane where $r_{12}$ changes sign, i.e., $r_{12} > 0$ below this line. This discards the entire lower curve shown in Fig. 13b. Furthermore, the snap-off value of the 12 AM $r_{12}^{\max} = 1.0$ poses a strong restriction. This restriction means that if the pressure in the phase 2 layer becomes too high, phase 2 will snap off bulk phase 1, before the intended 13 displacement can take place. Taking into account the 12 snap-off value, transformed in terms of $r_{13}$, as well as the 23 snap-off value, the remaining single valued part of the relation between $r_{13}$ and $r_{23}$ is presented in Fig. 9.

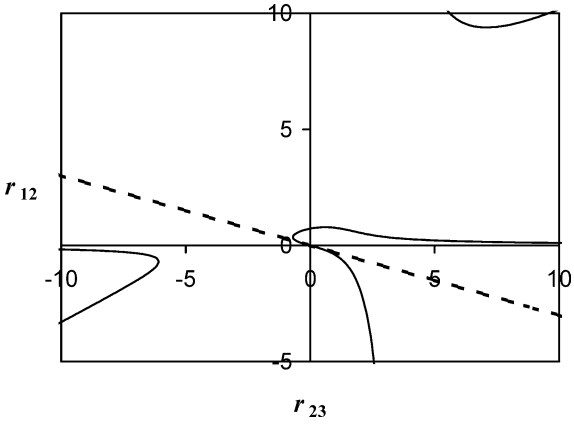


(a)

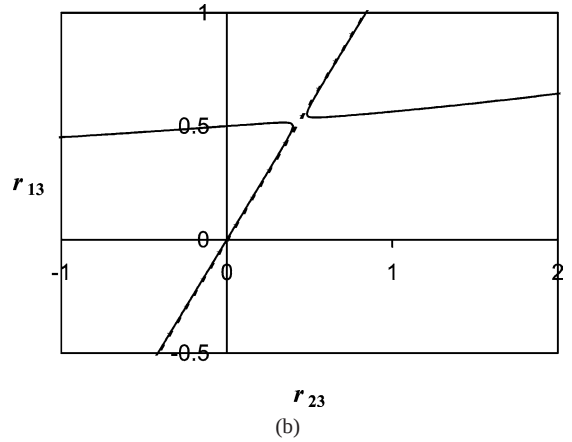


(b)

Fig. 13. Full relationship between two of the radii of curvature corresponding to piston-like displacement in an equilateral triangle for (a) phases 1 and 2 (Eq. (41)) with parameters of case 2 and (b) phases 1 and 3 (Eq. (43)) with parameters of case 1. The dashed lines indicate where the remaining third radius of curvature changes sign.

## References

[1] R.P. Mayer, R.A. Stowe, J. Colloid Interface Sci. 20 (1965) 893–911.
[2] H.M. Princen, J. Colloid Interface Sci. 30 (1969) 69–75.
[3] H.M. Princen, J. Colloid Interface Sci. 30 (1969) 359–371.
[4] H.M. Princen, J. Colloid Interface Sci. 34 (1970) 171–184.
[5] M. Lago, M. Araujo, J. Colloid Interface Sci. 243 (2001) 219–226.
[6] M. Lago, M. Araujo, Physica A 319 (2003) 175–187.
[7] M.I.J. van Dijke, K.S. Sorbie, J. Colloid Interface Sci. 260 (2003) 385–397.
[8] M. Dong, F.A.L. Dullien, I. Chatzis, J. Colloid Interface Sci. 172 (1995) 21–36.
[9] A.A. Keller, M.J. Blunt, P.V. Roberts, Transport Porous Media 26 (1997) 277–297.
[10] M. Sohrabi, G.D. Henderson, D.H. Tehrani, A. Danesh, in: Proceedings of the SPE Annual Technical Conference and Exhibition, Dallas, TX, October, 2000, SPE63000.
[11] D.H. Fenwick, M.J. Blunt, in: Proceedings of the 8th European Symposium on Improved Oil Recovery, Vienna, Austria, May, 1995.
[12] T. Firincioglu, M.J. Blunt, D. Zhou, Colloids Surf. A 155 (1999) 259–276.
[13] J. Lyklema, Fundamentals of Interface and Colloid Science, vol. 1, Fundamentals, Academic Press, London, 1991.

[14] M. Lago, R. Martin, M. Araujo, J. Colloid Interface Sci. 267 (2003) 429–444.
[15] F.E. Bartell, H.J. Osterhof, Ind. Eng. Chem. 19 (1927) 1277–1280.
[16] A.W. Adamson, Physical Chemistry of Surfaces, fifth ed., Wiley, New York, 1990.
[17] M.I.J. van Dijke, K.S. Sorbie, S.R. McDougall, Adv. Water Resour. 24 (2001) 365–384.
[18] T.C. Ransohoff, P.A. Gauglitz, C.J. Radke, AIChE J. 33 (1987) 753–765.
[19] S. Ma, G. Mason, N.R. Morrow, Colloids Surf. A 117 (1996) 273–291.